Realization of Vertical and Zigzag Single Crystalline Silicon Nanowire Architectures

V. A. Sivakov,*[,†] G. Brönstrup,[†] B. Pecz,[‡] A. Berger,[†,§] G. Z. Radnoczi,[‡] M. Krause,[∥] and S. H. Christiansen[†,⊥]

Institut für Photonische Technologien, Albert Einstein Str. 9, D-07745 Jena, Germany, MFA Hungarian Academy of Science, Konkoly Thege M. út 29-33, H-1121 Budapest, Hungary, Max Planck Institut für Mikrostrukturphysik, Weinberg 2, D-06120 Halle, Germany, Fraunhofer-Institut für Werkstoffmechanik IWM, Walter-Hülse-Str. 1, D-06120 Halle, Germany, and Max Planck Institut für die Physik des Lichts, Günther Scharowsky Str. 1, D-91054 Erlangen, Germany

Received: October 16, 2009; Revised Manuscript Received: January 25, 2010

Silicon nanowire (SiNW) ensembles with vertical and zigzag architectures have been realized using wet chemical etching of bulk silicon wafers (p-Si(111) and p-Si(100)) with a mask of silver nanoparticles that are deposited by wet electroless deposition. The etching of SiNWs is based on subsequent treatments in chemical solutions such as 0.02 M aqueous solutions of silver nitrate ($AgNO_3$) followed by 5 M hydrofluoric acid and 30% hydrogen peroxide (H_2O_2). The etching of the Si wafers is mediated by the reduction of silver on the silicon surface and in parallel by the oxidation of Si thereby forming SiO_2 which is dissolved in the HF surroundings. The morphology of the starting silver (Ag) layer/Ag nanoparticles that form during processing on the Si wafer surfaces strongly influences the morphology of the SiNW ensembles and homogeneity of the etch profile. Our observations suggest that the Ag layer/Ag nanoparticles not only catalyze the wet chemical etching of silicon but also strongly catalyze the decomposition of H_2O_2 so that the temperature of the etching solution substantially increases (strong exothermic reaction) and thus the etching velocity of bulk material. The morphology and microstructure of single crystalline SiNWs with respect to their crystallographic orientation was investigated by scanning (SEM) and transmission electron (TEM) microscopies and by electron backscatter diffraction (EBSD) in an SEM. Straight SiNWs as well as zigzag SiNWs can be realized depending on processing peculiarities. The optical characteristics such as absorption, transmission, and reflectance of the different silicon 1D architectures were investigated in an integrating sphere. Strong absorption and less reflection of visible and near-infrared light by the SiNW ensembles suggest that such material can be applied in the fields of opto-electronics, photonics and photovoltaics.

Introduction

In the last years, there is an enormously growing interest in the research and development of silicon nanowires (SiNWs) for various applications in the fields of opto-electronics, photonics, and photovoltaics as well as in the sensor field.[1–7] The silicon-based approaches are certainly favored due to material abundance and nontoxicity at a high level of materials control and understanding together with a huge industrial infrastructure to account for low production/processing costs and high production yields. The fabrication of SiNWs is based on either the metal catalyzed growth, known as vapor−liquid−solid growth (VLS),[8] where metal nanoparticles that form a low temperature eutectic with silicon, such as gold, are liquefied so that they form nanoscale droplets that can be supersaturated from the gas phase with silicon-containing species by, e.g., chemical vapor deposition (CVD) or physical vapor deposition methods[9] such as laser ablation, molecular beam epitaxy (MBE), or electron beam evaporation (EBE).[10–14] For all device concepts based on SiNWs, the crystal structure, geometry (alignment of SiNW with respect to the substrate), interfacial properties between the SiNW, and the substrate as well as the Si core and the SiO_2 shell of the SiNW (shell can either be native or thermally grown oxide), dopant concentrations and impurity levels are of key importance for functioning of the devices. For VLS-grown SiNWs the additional important question arises where and how much metal (gold) from the catalyst particle, that initiates the VLS[8] wire growth, resides in the SiNW.[15–17] However, the enormous impact that even smallest concentrations of Au as a dopant in silicon have a huge influence on opto-electronic properties of the SiNWs makes it essential to understand the extent to which Au atoms diffuse in the SiNW and Si(111) substrate and stay incorporated there and on the SiNW surfaces.[18] It has been shown that the Au from the catalyst is very mobile and diffuses all over the SiNW surfaces and between SiNWs at temperatures as low as 600 °C, leading to Ostwald ripening of Au nanoparticles at the NW sidewalls or even of the NW top Au droplet itself.[19–22] Alternatively, SiNWs can be realized by electroless wet chemical etching or electrochemical etching[23–29] into, e.g., bulk Si wafers or even thin silicon layers (they can be single-, multi-, nanocrystalline, or even amorphous) on substrates such as glass.[30]

In this paper we will report on the formation of SiNWs based on wet chemical etching making use of redox reaction processes of Ag layers/Ag nanoparticles and single crystalline silicon wafers (Si(111) and Si(100)) thereby obtaining a strong morphological control of the single crystalline SiNWs. In

* To whom correspondence should be addressed. Phone: +49(0)3641206440. Fax: +49(0)3641206499. E-mail: vladimir.sivakov@ipht-jena.de.
† Institut für Photonische Technologien.
‡ MFA Hungarian Academy of Science.
§ Max Planck Institut für Mikrostrukturphysik.
∥ Fraunhofer-Institut für Werkstoffmechanik IWM.
⊥ Max Planck Institut für die Physik des Lichts.

10.1021/jp909946x
Published on Web 02/11/2010

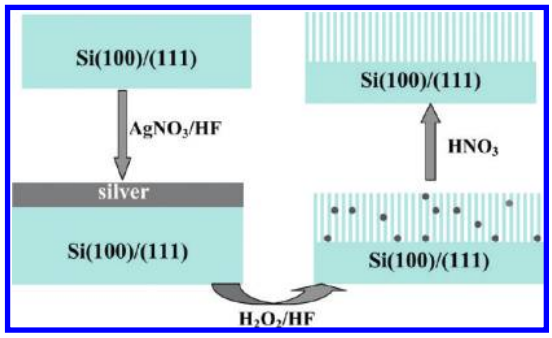

Figure 1. Schematic illustration of the etching process of silicon wafers using a sequence of two solutions; solution I is based on $AgNO_3$/HF (0.02 M $AgNO_3$/5 M HF), and solution II is based on H_2O_2/HF (30%H_2O_2/5 M HF in the volume ratio of 1:10). After solution I treatment, a quasicontinuous Ag layer forms (schematically indicated by a layer named silver) on the silicon surface consisting of densely aligning Ag nanoparticles.

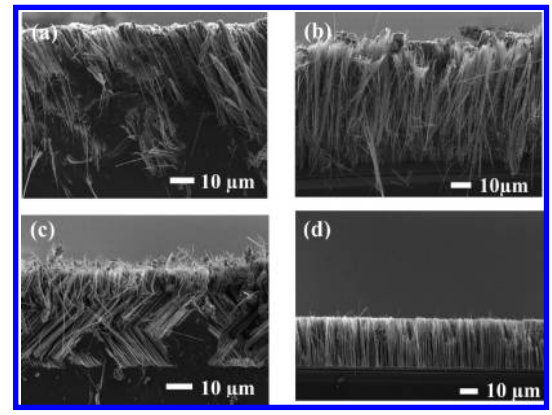

Figure 2. SEM cross-sectional micrographs of SiNW arrays formed *via* wet chemical treatment of Si(111) surfaces at: (a) **15s**, solution I; 1h, solution II; (b) **60s**, solution I; 1h, solution II; (c) **30s**, solution I; 1h, solution II. All etching experiments were performed using initial treatment in the 0.02 M $AgNO_3$ and 5 M HF (solution I) followed by 1h treatment in the second etching agent contained 30% H_2O_2 and 5 M HF in the volume ration of 1:10 (solution II); (d) SEM cross-sectional micrograph of SiNW arrays formed by 4h treatment of Si(111) wafer in 0.02 M $AgNO_3$ and 5 M HF solution as deduced from literature.[30]

comparison with other wet-chemical methods,[23–29] our proposed process has the advantage to be room temperature compatible, yielding SiNWs with lengths of more than 50 μm[31] and to be catalyst impurity free. The proposed etching process coincides with a strong detachment of thermal energy that can be explained as a byproduct of catalytic H_2O_2 decomposition on the Ag nanoparticle surfaces. The redox processing results in a strongly exothermic energy balance thereby enhancing the temperature of the etching solution quite substantially. The morphology and geometry of the SiNWs can be varied and thus the optical properties can be tuned by varying processing conditions and are discussed based on scanning electron microscopy (SEM) and transmission electron microscopies (TEM) studies.

Experimental Section

Boron-doped (0.7−20 Ωcm) 100 mm Si(111) and Si(100) oriented silicon wafers were used in the investigations. The silicon wafers were cleaned by rinsing in acetone for 2 min followed by an ethanol rinse for another 2 min. Native SiO_2 removal was carried out by a short dip in 40% hydrofluoric acid (HF) solution followed by a 2% HF rinse for 1 min. Finally, the samples were rinsed in deionized water and blow-dried with nitrogen. This cleaning procedure yields hydrogen-terminated silicon surfaces (for a limited time of a few minutes), which allowed for subsequent silver deposition on essentially oxide free silicon wafer surfaces. Our chemical etching method to produce SiNWs is based on a two-step process, as presented in Figure 1. In the first step, Ag nanoparticles were deposited on silicon wafer surfaces by immersing the wafers in aquaeous solution of 0.02 M silver nitrate ($AgNO_3$) and 5 M HF in the volume ratio 1:1 (solution I) for 15 to 60s. The morphology of the forming Ag nanoparticle deposits is strongly depending on the immersion time. In the second step, silicon wafers covered with Ag nanoparticles of different morphology were immersed in a 50 mL of second etching solution containing 5 M HF and 30% H_2O_2 in the volume ratio 10:1 (solution II) in a Teflon vessel for 1 h at room temperature. Finally the surfaces obtained after the etching procedures with solution I and II were rinsed several times in deionized water and dried at room temperature. The arrays were washed in a concentrated (65%) nitric acid (HNO_3) for 15 min to remove residual Ag nanoparticles from the SiNW surfaces. Structural analysis of the etched SiNWs has been carried out by field-emission SEM (FESEM, JEOL JSM-6300F) and TEM (FEI CM200/UT). The growth direction and crystal structure of etched SiNWs was investigated using electron backscatter diffraction (EBSD, TSL OIM 5/Digiview III mounted on a Zeiss Supra 55 VP SEM microscope). Combined with SEM, EBSD allows the determination of individual grain orientations, local textures, and point-to-point orientation correlations on bulk surfaces of polycrystalline materials.[32,33] EBSD studies are carried out on well-separated SiNWs that were isolated on copper TEM grids. This is done by detaching the SiNWs from the silicon substrate using ultrasonic treatment in alcohol and dropping of the SiNW suspension onto the TEM grid where the dilute SiNWs reside after evaporation of the alcohol. EBSD in the SEM at good pattern quality is carried out using an acceleration voltage of 15 kV and a probe current of approximately 2 nA. Optical characterization of ensembles of SiNWs was carried out in a UV−vis/NIR spectrometer (Perkin-Elmer Lambda 900) equipped with a 150 mm integrating sphere. Respective transmission (T) and reflectance (R) spectra were measured and a net internal absorption (A) has been calculated according to $R + T + A = 1$.

Results and Discussion

We show wet chemical etching of silicon wafers involving Ag nanoparticles, HF, and H_2O_2 to realize SiNWs of different morphologies depending on processing details, e.g., Ag nanoparticle morphology, silicon wafer orientation (Si(111) and Si(100)). With this control over morphologies at hand we can realize different optical properties of the material to be custom-made for optical/photonic devices such as, e.g., solar cells. The different SiNW morphologies were investigated using SEM as shown in Figure 2. SiNWs of different regularity and with different orientations could be obtained. Homogeneous etching profiles and thus regular SiNWs were observed for samples with thicker layers of silver nanoparticles, which form as a result of longer treatment in the $AgNO_3$/HF solution (solution I). On the basis of these micrographs, it becomes obvious that the silicon etching homogeneity is strongly depending on the morphology of the Ag nanoparticles/Ag layer. This finding is supported by TEM investigations (cf. Figure 3) that show how Ag nanoparticles/Ag layers reside on the silicon wafer surfaces after solution

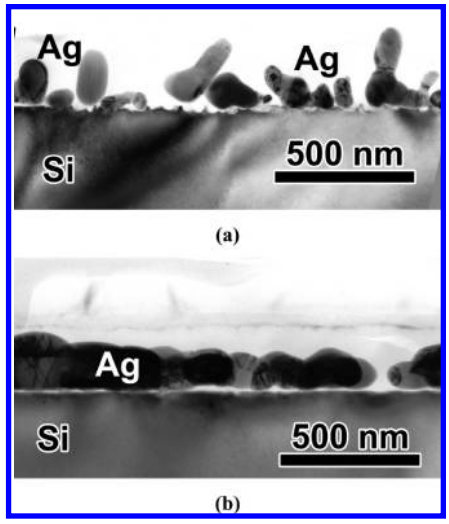

Figure 3. TEM cross-sectional micrographs of Ag nanoparticles on silicon wafer surfaces after solution I treatment (0.02 M $AgNO_3$/5 M HF) for: (a) 15s; (b) 30s.

I treatment, prior to solution II etching of SiNWs and also gives information about Ag/Si interface and crystallographic structure.

In Figure 3a, polycrystalline Ag nanoparticles are clearly visible residing on the p-Si(111) wafer surface after 15 s of treatment in solution I (0.02 M $AgNO_3$/5 M HF). After 30s of immersing in solution I an agglomeration of polycrystalline Ag grains on the p-Si(111) wafer surface is visible in Figure 3b. The TEM investigations show that the Ag nanoparticles are of odd shapes and are well separated (for <15 s treatment with solution I) and that they have direct contact with the silicon wafer surfaces. TEM investigations of Ag/Si surfaces show that elongated Ag grains contact the silicon wafer surfaces such that their long axis points parallel to the wafer surface. This may be a reason why the shorter treatment time (<15 s) in solution I results in a disordered etching profile as shown in Figure 2a. After a longer solution I treatment (>30 s) the Ag nanoparticles agglomerate and form quasicontinuous multicrystalline Ag layers (cf. Figure 3b), which may be the reason for a more homogeneous silicon etching profiles, as pointed out in parts b and c of Figure 2.

The SiNW arrays architecture strongly depends also on silicon wafer orientation. For comparison Si(100) and Si(111) wafers were etched under otherwise identical conditions, i.e., for 30 s in solution I followed by 1 h treatment in solution II (30% H_2O_2 and 5 M HF in the volume ratio of 1:10). Cross-sectional SEM images of SiNWs are shown in Figure 4, for p-Si(100) in Figure 4a and for p-Si(111) wafers in Figure 4b. Figure 4a shows straight SiNWs perpendicular to the wafer surface, as pointed out in previous papers.[23,34] The formation of SiNWs in Si(111) wafers appears to be more complicated (cf. Figure 2c, 4b), i.e., we can realize zigzag SiNW orientations, reproducibly. We can exclude that plastic deformation is responsible for this morphology based on TEM investigations that show the SiNWs to be free of extended defects such as dislocations or twins or stacking faults at the very edge of a zigzag SiNW (cf. Figure 4c).

To compare our results with existing literature data we can state the following: Chen et al. showed wet chemical etching to create SiNWs[34] using Si(100) and Si(110) wafers, and some of their results resemble our findings, i.e., they found preferential etching along [100] directions and for changing peculiarities of the etching conditions the Si(111) wafers could also etch along [111] directions, i.e., Si(111) wafers can either be etched perpendicular to the wafer surface along [111] direction or

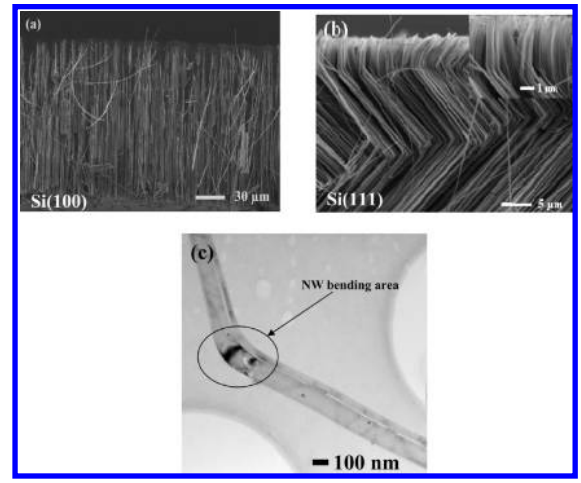

Figure 4. Electron microscopy investigations to show the influence of the starting Si wafer orientation on the SiNW arrays architectures (a) p-Si(100) wafer (0.7−1.5 Ω cm) cross-sectional SEM micrograph; (b) p-Si(111) wafer (1−20 Ω cm) cross-sectional SEM micrograph with inset of the zigzag close to the wafer surface; (c) TEM micrograph of two (a thin and a thick one) in parallel zigzag SiNW etched in the p-Si(111) wafer shown in the cross-sectional SEM micrograph (b); at the edge a bending contour is visible but now extended defects. The etching conditions were the same for both wafers: in the first step the wafers were treated with solution I (0.02 M $AgNO_3$ and 5 M HF in a volume ration 1:1) followed by 1 h treatment in solution II (30% H_2O_2 and 5M HF in a volume ration of 1:10).

pyramidal along [100] direction. We could show etching of Si(111) wafers for which we can realize straight (cf. parts b and d of Figure 2) etching along [111] directions or transition of [111] to [100] directions so that zigzag (cf. Figure 2c and 4b) architecture in SiNWs forms.

To prove the varying etching directions we used EBSD in SEM. Results of EBSD studies are shown in Figures 5 and 6. Because of its excellent spatial resolution of a few 10 nm even over large probed areas, EBSD enables orientation analysis of SiNW with emphasis on grain size (or single crystallinity), grain distribution, and SiNW orientations. Figure 5 proves single crystallinity over the full SiNW length, as given by the single color, coding the SiNW. In contrast to the common use of pole figures for orientation representation in the following the present crystal orientation will be illustrated by orientation cubes showing the orientation of the unit cell with respect to the sample surface. Here every orientation cube belongs to an individual point of the EBSD scan and thus provides only information for the particular point. According to that the determination of small deviations between different points could not be visualized, and no statistic about the entire scan could. Nevertheless it provides a direct visualization of the present crystal orientation and enables an intuitive access to the etching direction. Here it could be shown that etching SiNW from Si(100) wafer results in wires with a long axis almost parallel to the [100] direction.

The result of which is displayed by the color coding of the SiNW surface normal, which is a less important number since it shows only how the SiNW is lying on the TEM grid; thus, two SiNWs show different surface normal color coding in Figure 5 but identical [100] etching direction as well as the orientation cube that clearly shows the SiNW etching direction to be almost parallel to the [100] direction. In case of vertically etched SiNWs from Si(111) wafers the obtained etching direction is almost parallel to the ⟨111⟩ direction with uniform orientation. The overlayed orientation cube for this SiNW shows the etching direction to be close to [111]. Small deviations of the expected

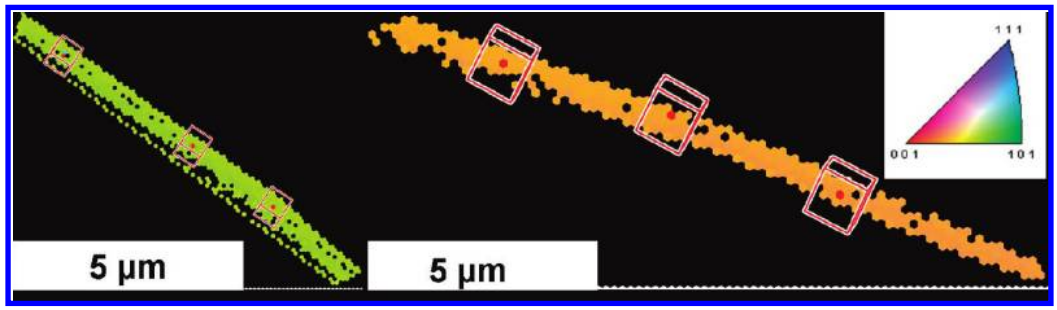

Figure 5. EBSD analysis (inverse pole figure representation) of two silicon nanorod (SiNR) fragments etched into a Si(111) wafer. The orientation cubes for both SiNWs show etching direction (parallel to the long axis of the SiNR) to be parallel to the [100] direction.

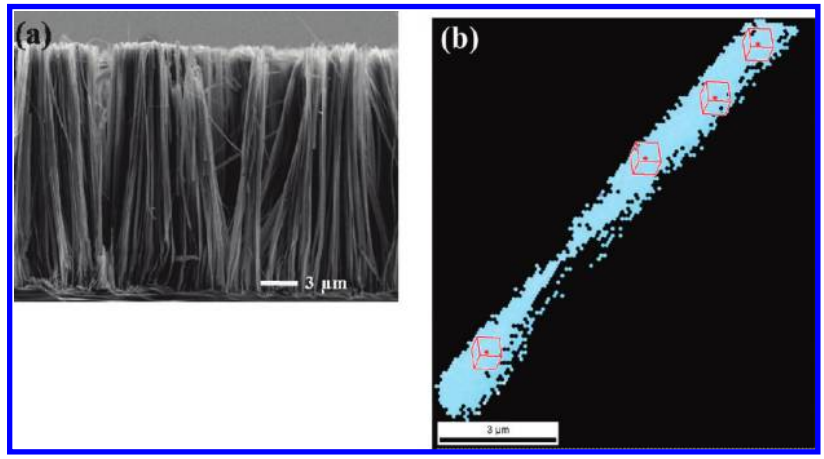

Figure 6. (a) SEM micrograph of vertically etched SiNWs into a Si(111) wafer; (b) EBSD analysis one SiNW fragment of such a wafer; color-coded inverse pole figure representation; the orientation cubes for this SiNW indicate etching direction (parallel to the long axis of the SiNW) to be parallel to the [111] direction.

crystal-directions could result from nonplanar positioning of the SiNW with respect to the TEM grid support. The cross-sectional SEM picture shows the straight SiNWs for this type of samples (cf. Figure 6a).

To support the understanding of the differences in etching morphologies that could be observed we carried out thermodynamic considerations of different processes. An interesting side effect of the solution I and solution II etching of silicon wafers was that the processes substantially lead to a heating of the etching solutions from initially room temperature to strongly elevated temperatures of 70 °C and above (depending on the used volumes of the solution). Our experiments show that in the first 10 min of etching in solution II (100 mL) the temperature of the solution reached 70 °C; after further 15 min of reaction time the temperature slowly decreased again reaching room temperature again after 1 h. One of the possible explanations of the energy release during the etching procedure in solution II is that a catalytic decomposition of H_2O_2 takes place. Haber and Weiss[35] have investigated the catalytic decomposition of H_2O_2 in homogeneous systems, where the H_2O_2, is primarily attacked monovalently, yielding the active radicals OH* or HO_2* (O_2^-) which may further give rise to the chain reactions as shown in eqs 1 and 2

$$OH^* + H_2O_2 = H_2O + HO_2^* \quad (1)$$

$$O_2^- + H_2O_2 = OH^- + OH^* + O_2\uparrow \quad (2)$$

The catalytic decomposition of H_2O_2 on Ag nanoparticles has also been studied by McIntosh[36] and Wiegel.[37] These groups have investigated the catalytic decomposition of H_2O_2 in the presence of colloidal Ag. The colloidal Ag partly dissolves in H_2O_2 without appreciable formation of gaseous components according to eqs 3 and 4

$$Ag + H_2O_2 = Ag^+ + OH^- + OH^* \quad (3)$$

$$Ag + OH^* = Ag^+ + OH^- \quad (4)$$

H_2O_2 is acting as an oxidizing agent in such an environment. Initially, the Ag surface is oxidized, but finally elemental Ag is formed again according to eq 5

$$Ag^+ + HO_2^- = Ag + HO^* \quad (5)$$

This reaction can take place to a considerable extent, so that elemental Ag and HO_2* radicals are produced. The latter starts the chain reactions of eqs 1 and 2 and give rise to a strong catalytic decomposition of the H_2O_2. As we pointed out in the experimental part, the etching process takes place in an acidic atmosphere by adding 5 M HF to the solution. In the case of decomposition in an acidic solution a smaller or greater part of the H_2O_2 is reduced to water without the formation of any gas, according to the equations taken from ref 38

$$H_2O_2 = H^+ = H_2O + OH^* + 61\ kcal \quad (6)$$

$$OH^* + H^+ = H_2O + 115\ \text{kcal} \quad (7)$$

As clearly seen from eqs 6 and 7 during catalytic decomposition of H_2O_2 on Ag nanoparticle surfaces in acidic atmosphere we have a strong exothermal reaction with substantial release of energy that can very well explain the heating of solution II in the first 10−15 min of the reaction followed by cooling back to room temperature once the H_2O_2 concentration decreases with reaction time. The substantial temperature rise in the initial 10−15 min of the process may very well influence the preferred etching directions. The thermodynamics and kinetic of etching process and influence of wafer nature to the etching process will be discussed in a separate paper.[39,40]

The stabilization and control of zigzag SiNW formation is very promising to be applied in optical/photonic applications.

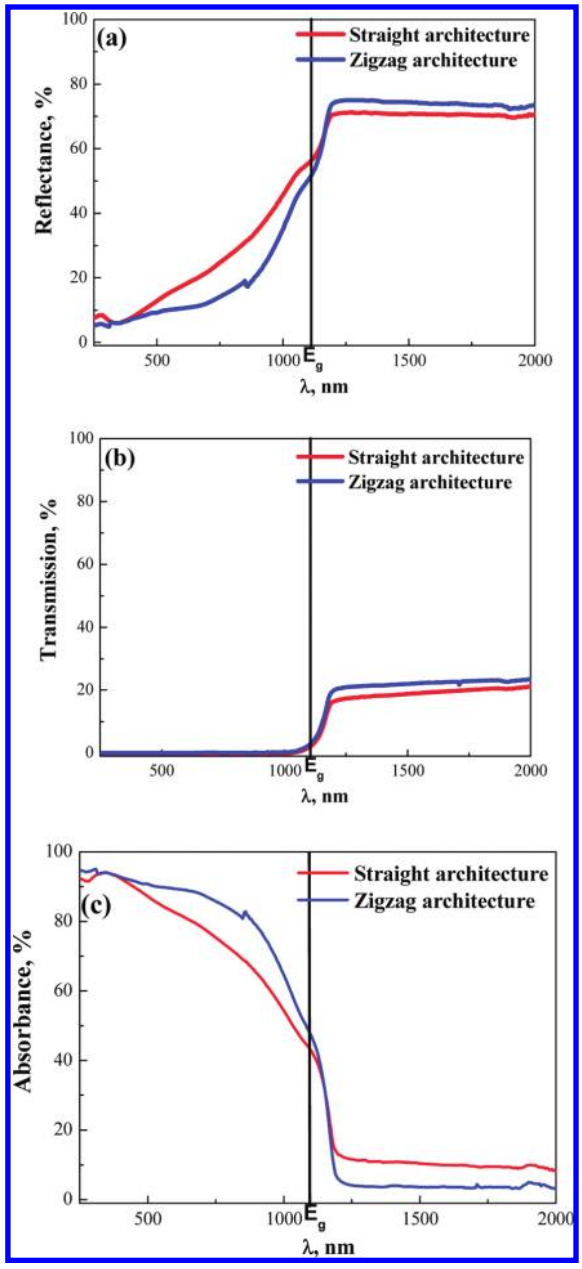

Figure 7. (a) Reflectance spectra of SiNW ensembles with straight and zigzag SiNWs architecture; (b) transmission spectra of SiNW ensembles with straight and zigzag SiNWs architecture; (c) absorbance spectra of SiNW ensembles with straight and zigzag SiNWs architecture. The solid line indicates the wavelength that corresponds to the Si band gap energy.

It appears to be obvious that straight and zigzag SiNWs show different optical properties such as scattering, absorption and transmission of light. Figure 7 shows the results of optical investigations of samples with straight and zigzag SiNWs using an integrating sphere. To obtain reliable and reproducible etching results a single side polished p-Si(111) wafer was used. All optical spectra were measured for light incidence perpendicular to the sample surface (up to 3° misalignment possible) using wavelengths from 400 to 2000 nm thereby covering the spectral regions above and below the Si band gap located at around 1100 nm (indicated by a black line in Figure 7). In the short wavelength range below 1100 nm the reflectance of etched SiNWs is in general low and depends on the morphology of SiNWs, i.e., zigzag SiNWs and straight SiNWs behave differently as visible from the curves in Figure 7. The transmission spectra show for short wavelengths (<1100 nm) very limited transmission for zigzag and straight, perpendicular to the surface SiNWs. Transmission values increase at higher wavelengths (>1100 nm) for both types of SiNWs architectures. The transmission behavior is important for the use of these SiNWs in antireflection coating applications or absorber layers both to be used e.g. for solar cells. The absorption behavior of the SiNW samples in Figure 7 is calculated from the reflection R and transmission T data, according to $R + T + A = 1$. The amount of absorbed light is significantly increased in the zigzag SiNW material, being important for the aforementioned absorber layer application. As we observed, the absorption of silicon material with zigzag architecture close to 1000 nm is over 60% and is thus higher than the absorption in the straight SiNWs.

Conclusions

We have demonstrated that we can realize homogeneously and reproducibly over large areas SiNW ensembles by wet chemical etching of Si wafers. Different SiNW architectures can be obtained by varying Si wafer orientation and processing peculiarities. Thus, we obtain SiNWs that can either be straight and perpendicular to the wafer surface with a preferred ⟨100⟩ direction of the SiNWs when using Si(100) starting wafers or zigzag with orientations varying between ⟨111⟩ and ⟨100⟩ directions when using Si(111) starting wafers. The etching process in acidic atmosphere is a strongly exothermic process thereby heating the etching solution substantially. This process inherent temperature rise is most probably responsible for the change in etching directions with time, thereby allowing the self-organized formation of zigzag SiNWs. The thermodynamics of the etching process and influence of wafer nature will be discussed in a separate paper.[39,40] All in all, zigzag and straight SiNWs show compared to a single crystalline wafers a strongly reduced reflectance and a strongly enhanced absorption. This may positively be used for optical devices such as, e.g., solar cells or photodetectors. For the strongly anisotropic zigzag SiNWs it should be interesting to perform angle dependent optical measurements, which are currently under way.

Acknowledgment. The authors gratefully acknowledge Mr. H. Köbe (Institute für Photonische Technologien, Jena/Germany) for the SEM investigations and to Mrs. S. Hopfe (Max Planck Institut für Mikrostrukturphysik, Halle/Germany) for the preparation of the TEM samples. The authors gratefully acknowledge financial support in part by the European Project in the framework of FP7, ROD-SOL, as well as by the Max-Planck-Society in the framework of the "nanostress" and EFRE, SiFasPB, projects. Pecz thanks the support of OTKA (Hungary) Project No. K75735.

References and Notes

(1) Cui, Y.; Lauhon, L. J.; Gudiksen, M. S.; Jianfang Wang, J.; Lieber, C. M. *Appl. Phys. Lett.* **2001**, *78*, 2214.

(2) Ross, F. M.; Tersoff, J.; Reuter, M. C. *PRL* **2005**, *95*, 146104.

(3) Hochbaum, A. I.; Fan, R.; He, R.; Yang, P. *Nano Lett.* **2005**, *5*, 457.

(4) Schmidt, V.; Senz, S.; Gösele, U. *Nano Lett.* **2005**, *5*, 931.

(5) Duan, X.; Huang, Y.; Cui, Y.; Wang, J.; Lieber, C. M. *Nature* **2001**, *409*, 66.

(6) Kelzenberg, M. D.; Turner-Evans, D. B.; Kayes, B. M.; Filler, M. A.; Putnam, M. C.; Lewis, N. S.; Atwater, H. A. *Nano Lett.* **2008**, *8*, 710.

(7) Stelzner, Th.; Pietsch, M.; Andrä, G.; Falk, F.; Ose, E.; Christiansen, S. H. *Nanotechnology* **2008**, *19*, 295203.

(8) Wagner, R. S.; Ellis, W. C. *Appl. Phys. Lett.* **1964**, *4*, 89.

(9) Wang, Y.; Schmidt, V.; Senz, S.; Gösele, U. *Nat. Nanotechnol.* **2006**, *1*, 186.

(10) Sivakov, V.; Heyroth, F.; Falk, F.; Andrä, G.; Christiansen, S. H. *J. Cryst. Growth* **2007**, *300*, 288.

(11) Sivakov, V.; Andrä, G.; Himcinschi, C.; Gösele, U.; Zahn, D. R. T.; Christiansen, S. *Appl. Phys. A: Mater. Sci. Process.* **2006**, *85*, 311.

(12) Fuhrmann, B.; Leipner, H. S.; Höche, H.-R.; Schubert, L.; Werner, P.; Gösele, U. *Nano Lett.* **2005**, *5*, 2524.

(13) Oh, S. H.; van Benthem, K.; Molina, S. I.; Borisevich, A. Y.; Luo, W.; Werner, P.; Zakharov, N. D.; Kumar, D.; Pantelides, S. T.; Pennycook, S. J. *Nano Lett.* **2008**, *8*, 1016.

(14) Kawashima, T.; Mizutani, T.; Nakagawa, T.; Torii, H.; Saitoh, T.; Komori, K.; Fujii, M. *Nano Lett.* **2008**, *8*, 1362.

(15) Wiethoff, C.; Ross, F. M.; Copel, M.; Horn-von Hoegen, M.; Meyer zu Heringdorf, F.-J. *Nano Lett.* **2008**, *8*, 3065.

(16) Bailly, A.; Renault, O.; Barrett, N.; Zagonel, L. F.; Gentile, P.; Pauc, N.; Dhalluin, F.; Baron, T.; Chabli, A.; Cezar, J. C.; Brookes, N. B. *Nano Lett.* **2008**, *8*, 3709.

(17) Putnam, M. C.; Filler, M. A.; Kayes, B. M.; Kelzenberg, M. D.; Guan, Y.; Lewis, N. S.; Eiler, J. M.; Atwater, H. A. *Nano Lett.* **2008**, *8*, 10.

(18) Allen, J. E.; Hemesath, E. R.; Perea, D. E.; Lensch-Falk, J. L.; Li, Z. Y.; Yin, F.; Gass, M. H.; Wang, P.; Bleloch, A. L.; Palmer, R. E.; Lauhon, L. J. *Nat. Nanotechnol.* **2008**, *3*, 16.

(19) Ostwald, W. *Z. Phys. Chem.* **1900**, *34*, 495.

(20) Wagner, C. Z. *Elektrochem.* **1961**, *65*, 581.

(21) Lifschitz, I. M.; Slyozov, V. V. *Phys. Chem. Solids* **1981**, *19*, 35.

(22) Hannon, J. B.; Kodambaka, S.; Ross, F. M.; Tromp, R. M. *Nature* **2006**, *440*, 69.

(23) Peng, K. Q.; Yan, Y. J.; Gao, S. P.; Zhu, J. *Adv. Mater.* **2002**, *14*, 1164.

(24) Huang, Z.; Zhang, X.; Reiche, M.; Liu, L.; Lee, W.; Shimizu, T.; Senz, S.; Gösele, U. *Nano Lett.* **2008**, *8*, 3046.

(25) Peng, K. Q.; Wu, Y.; Fang, H.; Zhong, X. Y.; Xu, Y.; Zhu, J. *Angew. Chem., Int. Ed.* **2005**, *44*, 2737.

(26) Peng, K. Q.; Hu, J. J.; Yan, Y. J.; Wu, Y.; Fang, H.; Xu, Y.; Lee, S. T.; Zhu, J. *Adv. Funct. Mater.* **2006**, *16*, 387.

(27) Qiu, T.; Wu, X. L.; Yang, X.; Huang, G. S.; Zhang, Z. Y. *Appl. Phys. Lett.* **2005**, *84*, 386.

(28) Peng, K.; Zhang, M.; Lu, A.; Wong, N. B.; Zhang, R.; Lee, S. T. *Appl. Phys. Lett.* **2007**, *90*, 163123.

(29) Fang, H.; Wu, Y.; Zhao, J.; Zhu, J. *Nanotechnology* **2006**, *17*, 3768.

(30) Sivakov, V.; Andrä, G.; Gawlik, A.; Berger, A.; Plentz, J.; Falk, F.; Christiansen, S. H. *Nano Lett.* **2009**, *9*, 1549.

(31) Hochbaum, A. I.; Chen, R.; Diaz Delgado, R.; Liang, W.; Garnett, E. C.; Najarian, M.; Majumdar, A.; Yang, P. *Nature* **2008**, *451*, 163.

(32) Randle, V. Theoretical framework for electron backscatter diffraction. In *Electron backscatter diffraction in material science*; Kluwer Academic: Dordrecht, 2000.

(33) Isabell, T. C. *Ultramicroscopy* **1997**, 67.

(34) Chen, C.-Y.; Wu, C.-S.; Chou, C.-J.; Yen, T.-J. *Adv. Mater.* **2008**, *20*, 3811.

(35) Haber, F.; Weiss, J. *Proc. Roy. Soc.* **1934**, *147A*, 332.

(36) McIntosh, D. M. *J. Phys. Chewz.* **1902**, *6*, 15.

(37) Wiegel, B. *Z. Phys. Chem.* **1929**, *143A*, 81.

(38) Weiss, J. *Trans. Faraday Soc.* **1935**, *31*, 1547.

(39) Sivakov, V. A.; Berger, A.; Dellith, A.; Christiansen, S. H. Unpublished results.

(40) Sivakov, V. A.; Voigt, F.; Berger, A.; Bauer, G.; Christiansen, S. H. Roughness of Silicon Nanowire Sidewalls: the Key to Understand Room Temperature Photoluminescence submitted to *Nano Lett.* 2010.

JP909946X